Electronic Supplementary Material (ESI) for Nanoscale.

Supporting information

Atomic Structure and Formation Mechanism of Sub-Nanometer Pores in 2D Monolayer MoS_2

Shanshan Wang[1], Huashan Li[2], Hidetaka Sawada[1,3,4], Christopher S. Allen,[1,4] Angus I. Kirkland[1,4], Jeffrey C. Grossman[2], Jamie H. Warner[1]**

[1]Department of Materials, University of Oxford, Parks Road, Oxford, OX1 3PH, United Kingdom

[2]Department of Materials Science and Engineering, Massachusetts Institute of Technology, 77 Massachusetts Avenue, Cambridge, MA, 02139, USA.

[3]JEOL Ltd., 3-1-2 Musashino, Akishima, Tokyo 196-8558, Japan

[4]Electron Physical Sciences Imaging Center, Diamond Light Source Ltd, Didcot, Oxfordshire, OX11 0DE, United Kingdom

Email: *Jamie.warner@materials.ox.ac.uk; jcg@mit.edu

S1. Raw images showing nanopore formation procedure in figure 3

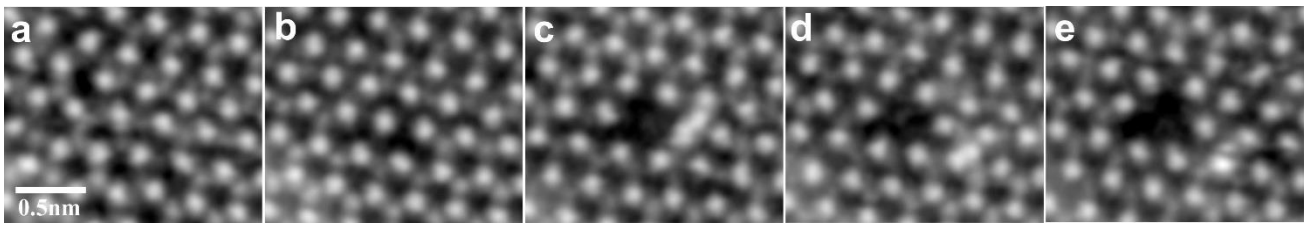

Figure S1. Raw ADF-STEM image series of Figure 3j to m showing nanopore formation dynamics.

S2. Raw images showing nanopore formation dynamics in figure 4

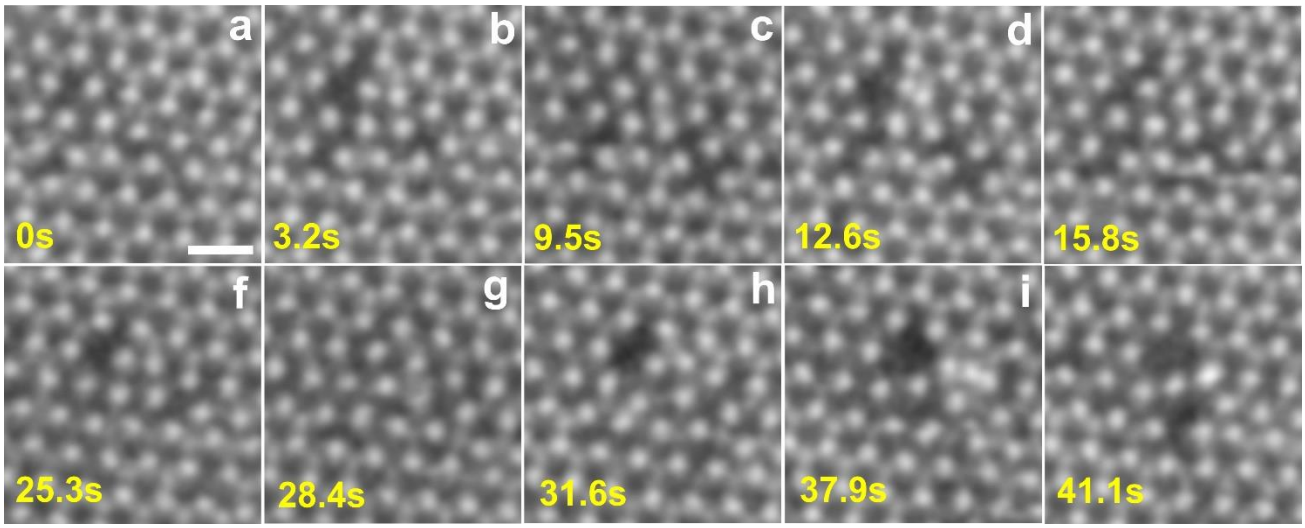

Figure S2. Time series of ADF-STEM images of figure 4 (i) without labels. The scale bar corresponds to 0.5 nm.

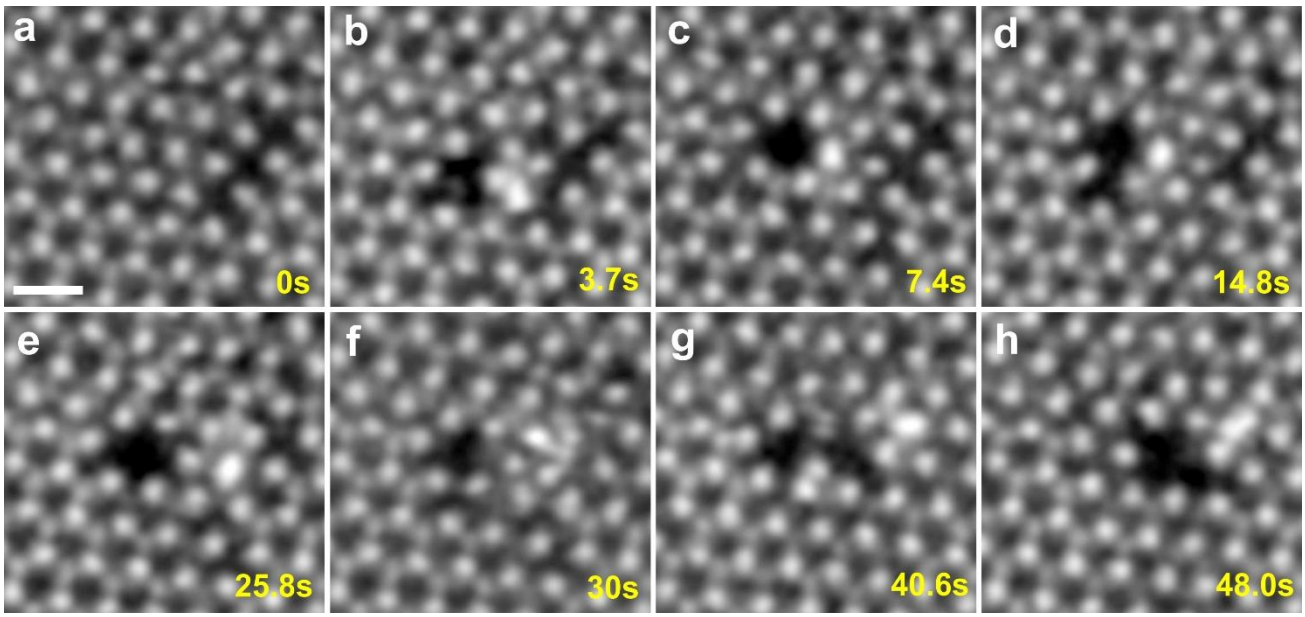

Figure S3. Time series of ADF-STEM images of figure 4 (ii) without labels. The scale bar corresponds to 0.5 nm.

S3. Drilling of nanopore arrays and their stability

Here we show that our drilling approach for nanopore arrays at 80 kV. Slow scan rates and drill times of 30s were used to produce nanopores that were between 0.7-1.2nm in diameter. Figure S4a shows the clean area of MoS_2 used for the patterning and figure S4b shows the same area after drilling four nanopores in cross pattern. After drilling and then imaging these four nanopores, we then drilled a further four more nanopores into the same structure to produce the 2D patterned array in figure S4d. These nanopores are regularly spaced with distances of ~4-5nm. A higher magnification image of the top nanopore in figure S4b, is presented in figure S4c to show the details of the structure. Again, Mo edge termination is dominant and Mo atoms are found on the surface next to the nanopore. The diameter of the nine pores in figure S4 are relatively uniform and show the control over both the pitch and diameter of the holes.

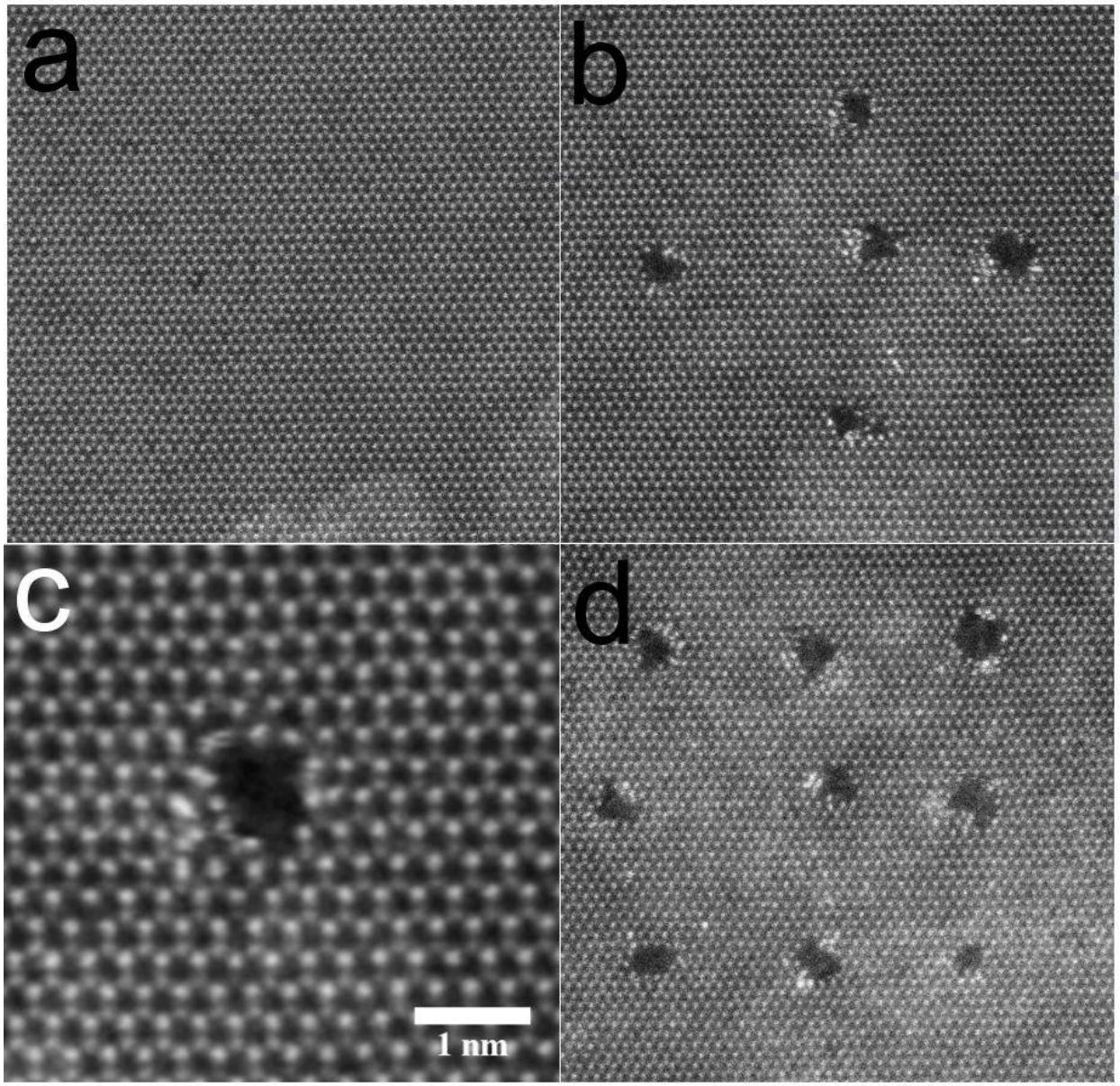

Figure S4. Drilling 2D patterns of nanopores in MoS2 with 30s exposure time. (a) Pristine MoS_2 area used for drilling experiments. (b) Four nanopores drilled into MoS_2 with cross pattern using 30s exposure times and then imaging with faster scan rate. (c) High magnification image of the top nanopore in (b). (d) Another four nanopores added to the original structure in (b) by sequential 30s drilling.

Figure S5 shows the same area after sequential ADF-STEM imaging to demonstrate the stability of the nanopores after creating and during post-creation rapid scan imaging.

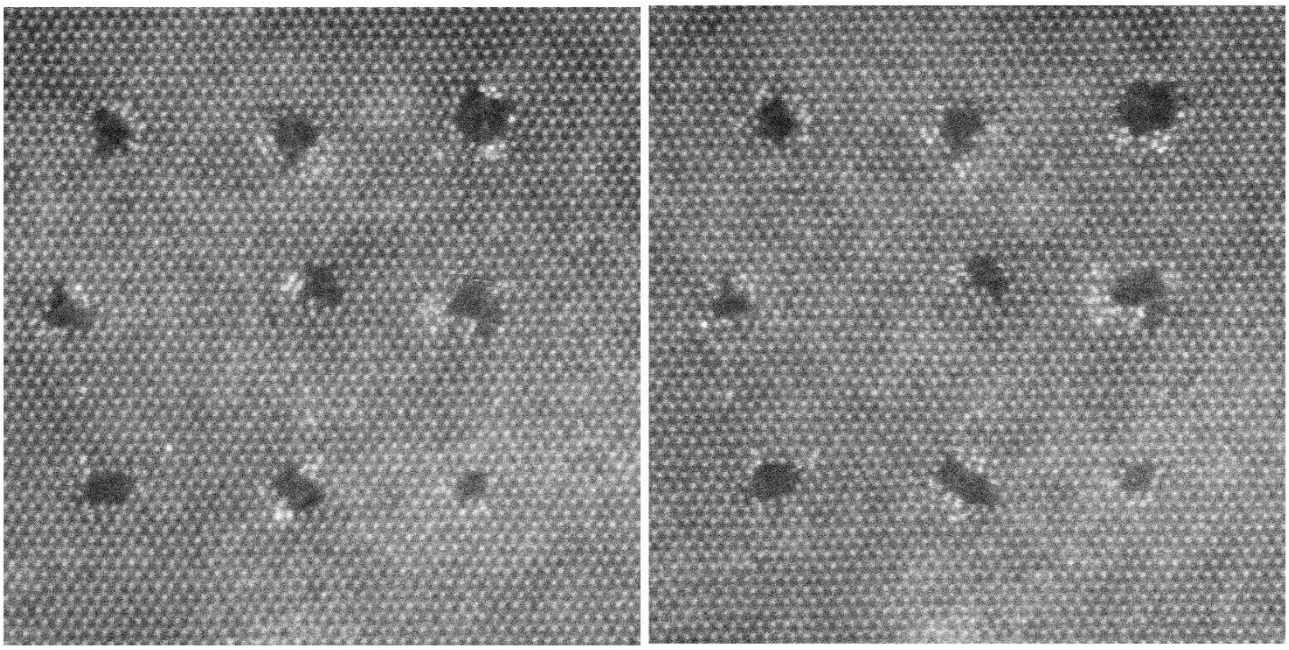

Figure S5. Two sequential images taken of the nanopore array to show the stability.

S4. Demonstration of resolution.

Figure S6(a) shows the FFT from figure 5d with spots extending out to 0.09nm. False colour with ‘fire’ LUT is to improve the visual inspection of the spots in the FFT. A line profile, shown in figure S6(b), was taken across the spots to reveal the peaks associated with 0.27nm, 0.13nm and 0.09nm (figure S6(c)).

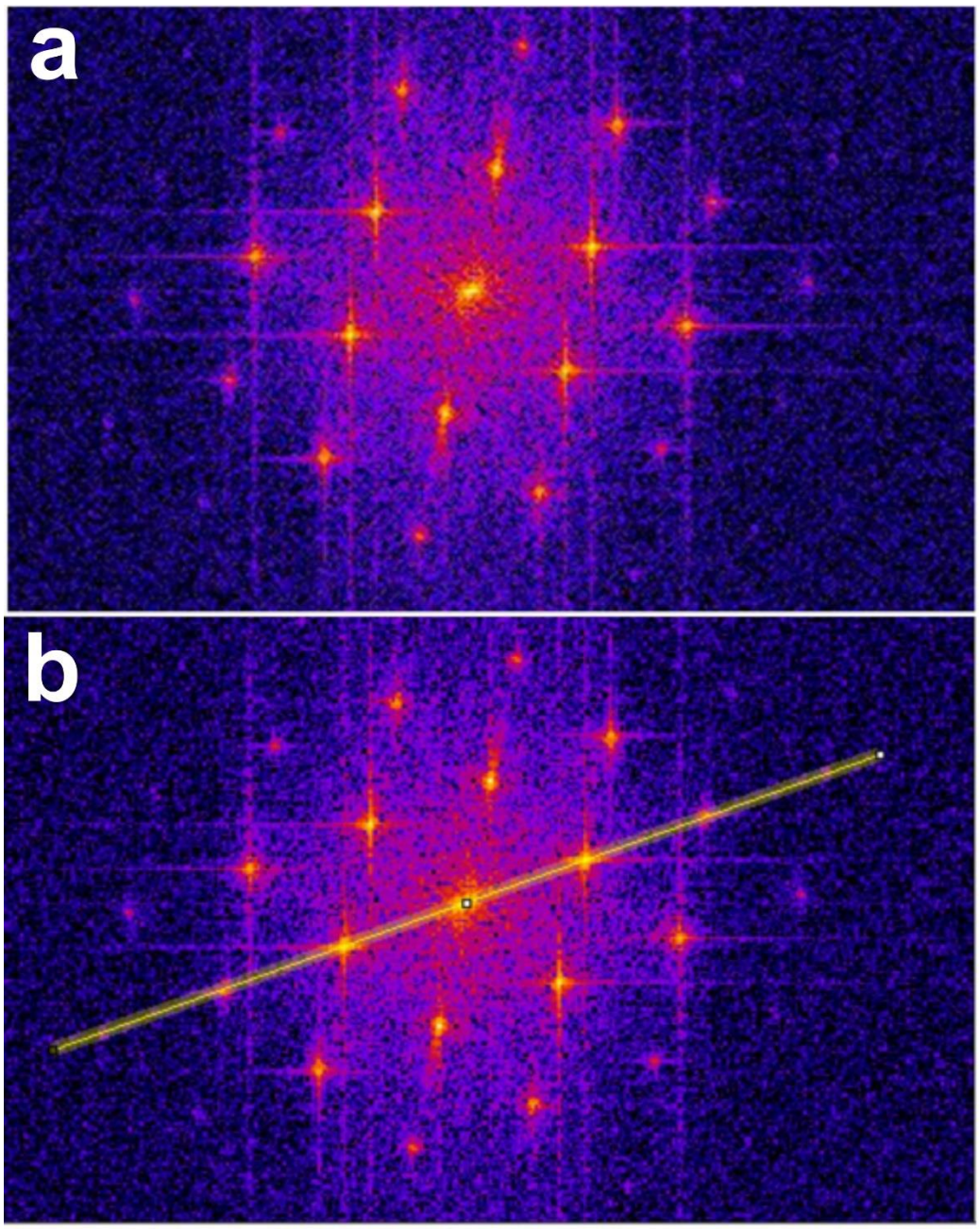
a
b
c
0.27nm
0.13nm
0.09nm
Gray Value
150
100
50
0.0
0.5
1.0
1.5
1/distance (a.u)

Figure S6. (a) FFT from figure 5d. (b) Showing the region for a line profile analysis. (c) Line profile showing the spots associated with 0.27nm, 0.13nm and 0.09nm are present in the FFT.

S5. Stability of nanopores losing 1 Mo and its neighbouring 12 S atoms from DFT calculations

We also conducted DFT calculations for the nanopore composed of a single Mo atom with its surrounding 12 sulphur atoms. Figure S7 (a)–(e) shows 5 initial structures of the nanopore with their corresponding DFT-calculated final configurations shown in panel (f)–(j). As depicted in Figure S7 (i), having the ejected Mo atom attached to locations close to the nanopore edge and cluster with those sub-coordinated Mo atoms is the most energetically preferable, while residing the ejected Mo atom on top of the Mo lattice site far away from the nanopore is the most unstable, which is consistent with the DFT calculation results for the nanopore composed of a single Mo atom and its coordinated 6 sulphur atoms in figure 6. The nanopore potential profile for this type of nanopore configuration is also very sensitive to the local structure when the ejected Mo atom is close to the nanopore, agreeing well with figure 6 (j) and (k).

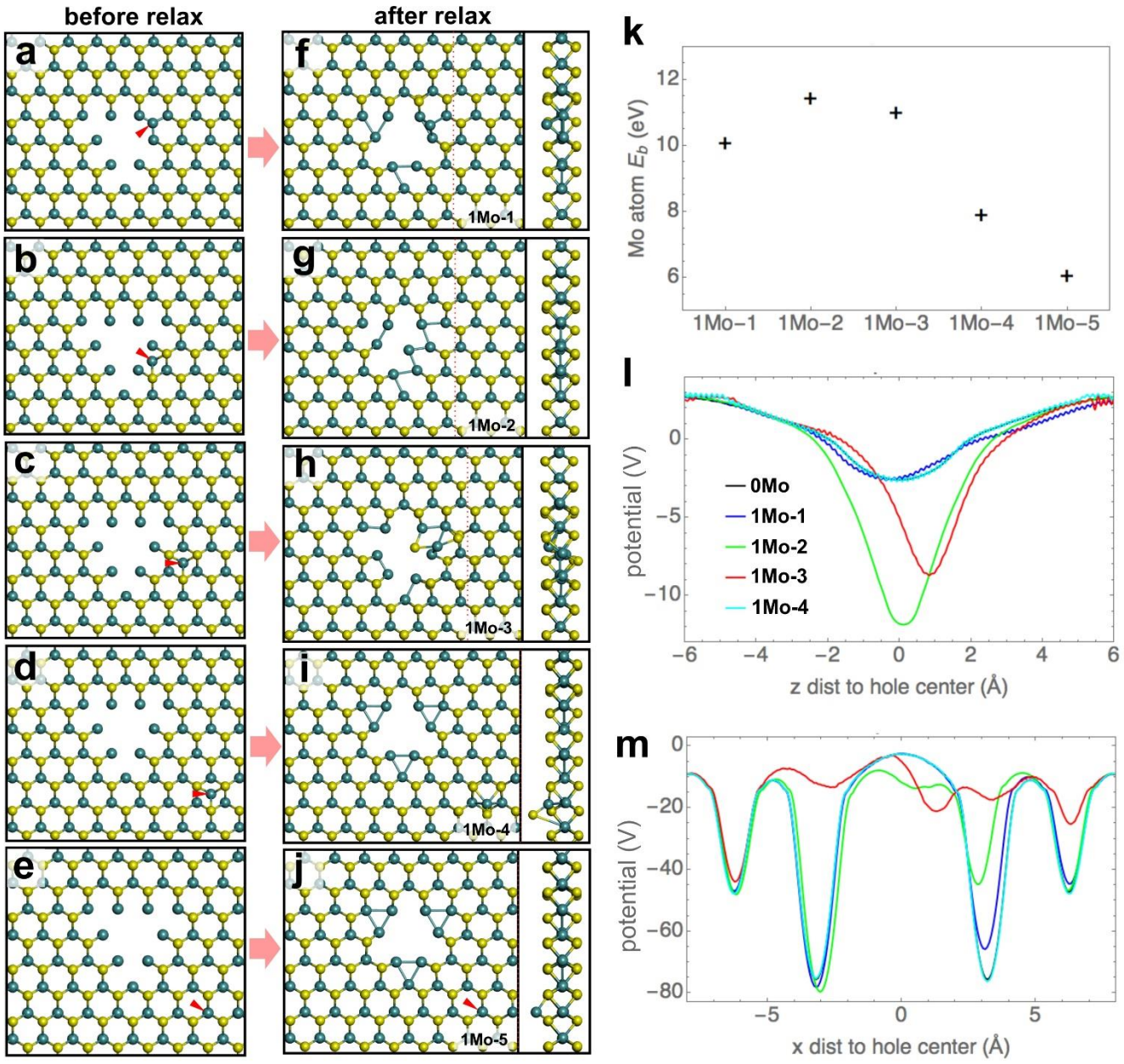

Figure S7. DFT calculations showing the energetically favourable structures of the nanopore composed of a single Mo atom and its neighbouring 12 sulphur atoms. (a–e) initial and (f-j) final structures of geometry optimization for the 5 different possible configurations of the nanopore, with the red arrows indicating the positions of the ejected Mo atom. Side views from the cross sections marked by the red dashed lines are shown on right panels. (i) The site dependent binding energies of the ejected Mo atom on the sheet surface. (j-k) The potential profile of the nanopores as a function of the distance between the ejected Mo atom and the hole centre along the z direction and the x

direction, respectively. The 0 Mo denotes the nanopore by itself assuming the ejected Mo atom has escaped from the surface, while the remaining legends are consistent with panel a-j.

S6. DFT-calculated configuration evolution of the MoS_2 sub-nanometre pore as a function of the relaxation step corresponding to figure 3n

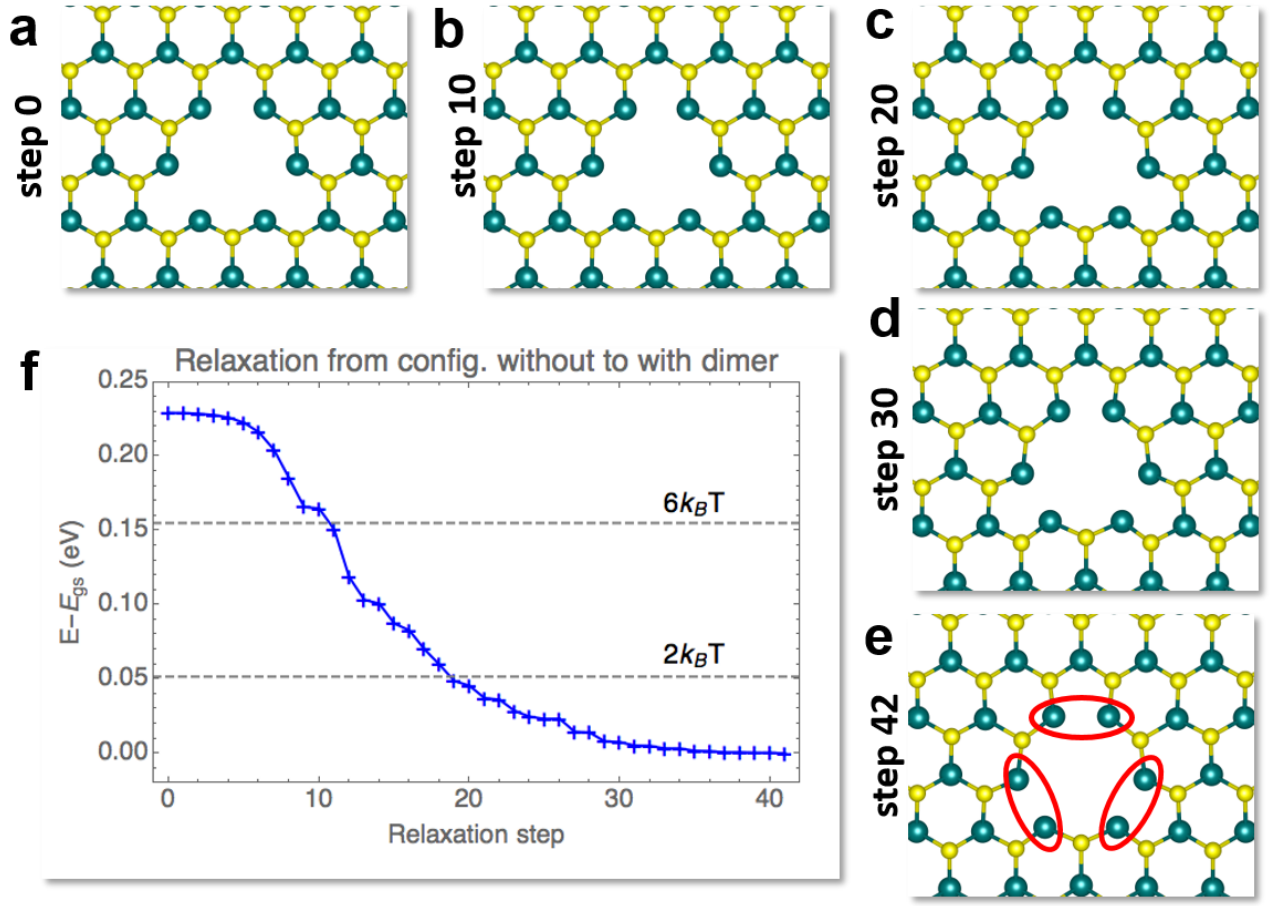

Figure S8. (a-e) DFT-calculated models showing configurations of the MoS_2 nanopore at different relaxation steps. (f) Plot showing the energy difference contributed by each Mo dimer compared to the ground state as a function of the relaxation step. The Mo dimers are marked by red ovals in panel e.

We tracked the DFT-calculated sub-nanometre nanopore structure evolution as the relaxation step increases (figure S8 a-e). The initial state was chosen to be the relaxed nanopore configuration with the 6 Mo atoms surrounding the hole frozen in positions at pristine sheet. Then the constraint was released for

further geometric optimization, and the convergence criterion was met at the 42nd step. Figure S8f is the plot showing (E-E_{gs}) changes as a function of the relaxation step. E-E_{gs} is defined as the energy difference contributed by each Mo dimer (total/3) compared to the ground state. We can see that the dimerized configuration is energetically more favourable than the one without Mo dimers, but the energy difference (0.23 eV per dimer) is kind of comparable to thermal fluctuation (several k_BT). With an energy penalty of 0.15 eV (step 10), the degree of dimerization can be significantly reduced. In addition, as depicted in figure S8f, there is no barrier between these two states. Therefore, the sub-nanometre pore structure observed in figure 3n, which do not show Mo atoms dimerized, could be attributed to the thermal fluctuation, making the configuration switch between dimerized and undimerized Mo atoms on edges to be relatively easy to take place in reality.

S7. Drilling larger nanopores in MoS2

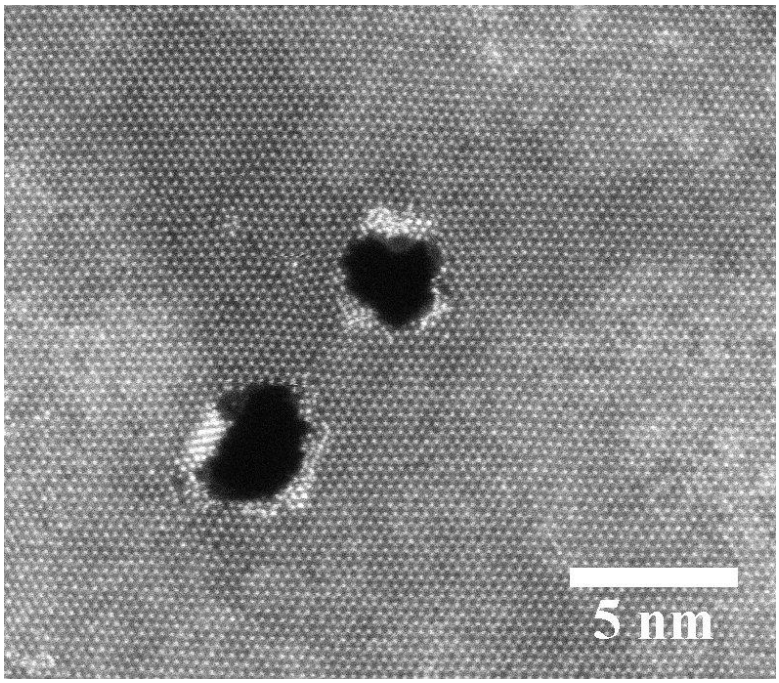

Figure S9. Drilling of two larger 3-4nm holes next to each other in monolayer MoS_2 using larger scan area.

S8. Formation energies of nanopores

The formation energy of the nanopore is defined as

$$E_{form} = N_s E_s + N_{mo} E_{mo} + E_{pore} - E_{mos2}$$

Where E_{pore} is the energy of the nanopore structure, E_{mos2} is the energy of the pristine MoS_2 monolayer, $N_{s/mo}$ is the numbers of ejected S/Mo atoms, and $E_{s/mo}$ is the energy of an isolated S/Mo atom in the corresponding unit cell. Our calculated formation energy of an S vacancy is 6.9 eV, which is consistent with literature.[1] The formation energies of the nanopores studied in this work are summarized in Table S1.

Table S1. Formation energies of nanopores with various configurations. The notation xmov-ysv-zmot means the system contains x Mo vacancies, y S vacancies and z Mo atoms on top of the sheet, and the labels of the configurations are consistent with those in Figure 6 and Figure S7.

Configurations	E_{form} (eV)
1mov-6sv	54.9
1mov-6sv-1mot.cf1	42.9
1mov-6sv-1mot.cf2	44.6
1mov-6sv-1mot.cf3	47.0
1mov-6sv-1mot.cf4	48.4
1mov-12sv	97.6
1mov-12sv-1mot.cf1	87.5
1mov-12sv-1mot.cf2	86.2
1mov-12sv-1mot.cf3	86.6
1mov-12sv-1mot.cf4	89.7
1mov-12sv-1mot.cf5	91.5

S9. Impact of spin polarization

While spin-polarized calculations are necessary to accurately predict the electronic properties, the impact of spin-polarization is relatively small for close-shell systems without dopants, even in the presence of Mo and S vacancies as illustrated by previous studies.[2] This is also verified by our simulations on the 1Mo-2 structure shown in Figure 6, wherein the difference between the total energies computed with and without spin polarization is 0.1 eV, much smaller than the energy variations caused by different configurations (about 6 eV as shown in Figure 6 (i) and Figure S7 (k)). In addition, we confirmed that the incorporation of spin polarization effects only slightly changes the potential profiles along both the directions parallel and perpendicular to the sheet (Figure S10, S11).

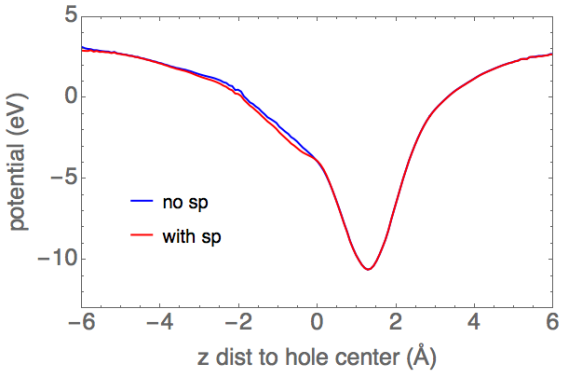

Figure S10. The potential profile of the nanopore (1Mo-2 structure in Figure 6) as a function of the distance between the ejected Mo atom and the hole center along the z direction, obtained by DFT simulations with (in red) and without (in blue) spin polarization.

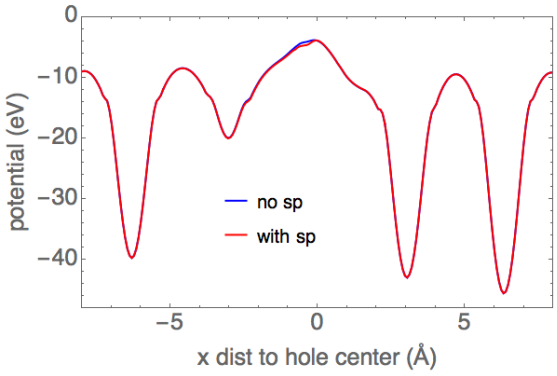

Figure S11. The potential profile of the nanopore (1Mo-2 structure in Figure 6) as a function of the distance between the ejected Mo atom and the hole center along the x direction, obtained by DFT simulations with (in red) and without (in blue) spin polarization.

References

1 H.-P. Komsa, J. Kotakoski, S. Kurasch, O. Lehtinen, U. Kaiser and A. V. Krasheninnikov, *Phys. Rev. Lett.*, 2012, **109**, 035503.

2 Y. C. Cheng, Z. Y. Zhu, W. B. Mi, Z. B. Guo and U. Schwingenschlögl, *Phys. Rev. B*, 2013, **87**, 100401.